



The Deubiquitinase USP13 Maintains Cancer Cell Stemness by Promoting FASN Stability in Small Cell Lung Cancer

Juhong Wang^{1,2}, Weihao Lin^{1,2}, Renda Li^{1,2}, Hong Cheng^{1,2}, Sijin Sun^{1,2}, Fei Shao³, Yannan Yang^{1,2}, Lin Zhang^{1,2}, Xiaoli Feng⁴, Shugeng Gao¹, Yibo Gao^{1,2,3*} and Jie He^{1,2*}

¹ Department of Thoracic Surgery, National Cancer Center/National Clinical Research Center for Cancer/Cancer Hospital, Chinese Academy of Medical Sciences and Peking Union Medical College, Beijing, China, ² State Key Laboratory of Molecular Oncology, National Cancer Center/National Clinical Research Center for Cancer/Cancer Hospital, Chinese Academy of Medical Sciences and Peking Union Medical College, Beijing, China, ³ Laboratory of Translational Medicine, National Cancer Center/National Clinical Research Center for Cancer/Cancer Hospital, Chinese Academy of Medical Sciences and Peking Union Medical College, Beijing, China, ⁴ Department of Pathology, National Cancer Center/National Clinical Research Center for Cancer/Cancer Hospital, Chinese Academy of Medical Sciences and Peking Union Medical College, Beijing, China

OPEN ACCESS

Edited by:

Paul Takam Kamga,
Université de Versailles
Saint-Quentin-en-Yvelines, France

Reviewed by:

Wei Yang,
Cedars Sinai Medical Center,
United States
Ren-Wang Peng,
Bern University Hospital, Switzerland

*Correspondence:

Yibo Gao
gaoyibo@cicams.ac.cn
Jie He
hejie@cicams.ac.cn

Specialty section:

This article was submitted to
Cancer Metabolism,
a section of the journal
Frontiers in Oncology

Received: 19 March 2022

Accepted: 20 June 2022

Published: 11 July 2022

Citation:

Wang J, Lin W, Li R, Cheng H,
Sun S, Shao F, Yang Y, Zhang L,
Feng X, Gao S, Gao Y and He J
(2022) The Deubiquitinase USP13
Maintains Cancer Cell Stemness
by Promoting FASN Stability in
Small Cell Lung Cancer.
Front. Oncol. 12:899987.
doi: 10.3389/fonc.2022.899987

USP13 is significantly amplified in over 20% of lung cancer patients and critical for tumor progression. However, the functional role of USP13 in small cell lung cancer (SCLC) remains largely unclear. In this study, we found that the deubiquitinase USP13 is highly expressed in SCLC tumor samples and positively associated with poor prognosis in multiple cohorts. *In vitro* and *in vivo* depletion of USP13 inhibited SCLC cancer stem cells (CSCs) properties and tumorigenesis, and this inhibitory effect was rescued by reconstituted expression of wide type (WT) USP13 but not the enzyme-inactive USP13 mutant. Mechanistically, USP13 interacts with fatty acid synthase (FASN) and enhances FASN protein stability. FASN downregulation suppresses USP13-enhanced cell renewal regulator expression, sphere formation ability, and *de novo* fatty acids biogenesis. Accordingly, we found FASN expression is upregulated in surgical resected SCLC specimens, positively correlated with USP13, and associated with poor prognosis of SCLC patients. More importantly, the small molecule inhibitor of FASN, TVB-2640, significantly inhibits lipogenic phenotype and attenuates self-renewal ability, chemotherapy resistance and USP13-mediated tumorigenesis in SCLC. Thus, our study highlights a critical role of the USP13-FASN-lipogenesis axis in SCLC cancer stemness maintenance and tumor growth, and reveals a potential combination therapy for SCLC patients.

Keywords: USP13, cancer stem cells, FASN, ubiquitylation, lipogenesis, TVB-2640, SCLC

Abbreviations: SCLC, Small-cell lung cancer; CSC, Cancer stem-like cell; USP13, Ubiquitin-specific peptidase 13; FASN, Fatty acid synthase; TMA, Paraffin-embedded tissue microarray; HR, hazard ratio; shRNA, Short hairpin RNA; DUB, Deubiquitinating-enzyme; Ub, Ubiquitin; USPs, Ubiquitin-specific proteases; WT, Wild type; IP, Immunoprecipitation; CHX, Cycloheximide; IHC, Immunohistochemistry; qRT-PCR, Real-time quantitative reverse transcriptase-polymerase chain reaction; MS, Mass spectrometry; OS, Overall survival.

INTRODUCTION

Small-cell lung cancer (SCLC) is a neuroendocrine (NE), early metastatic, rapidly progressing and therapy-resistant lung cancer, with 5-year survival of 15%–30% for limited-stage disease, and less than 1% for patients with extensive-stage disease according to the Veteran Affairs Lung Group staging criteria (1–3). Although the sequencing results have provided a better understanding of the signaling pathways in SCLC, most recurrent genetic events are not directly linked to obvious regulatory network. Recently, proteomic analyses revealed other putative vulnerabilities that eventually led to the identification of improved therapeutic strategies (4–6), suggesting the importance of identifying targetable proteins that directly contribute to tumor development or drug resistance. Cancer stem cells (CSCs) in SCLC play a central role in tumorigenesis, metastasis, drug resistance and recurrence (7–9). Convincing evidences demonstrated that substantial post-translational heterogeneity exists within cancer cells can affect characteristics of cancer cell stemness (10–12). Therefore, the exploration of intracellular important post-translational regulatory signaling pathways can provide a promising targetable strategy for tumor treatment.

Protein ubiquitination, post-translational modification that regulates all kinds of cellular biological processes, is counteracted upon deubiquitylation by deubiquitinating enzymes (DUBs). DUBs played crucial role in CSC maintenance and differentiation through the regulation of core stem cell transcription factors (SCTFs), such as Oct4, Nanog, and the stem cell surface marker CD133 along with cancer cell sphere formation ability (13–16). In more than one hundred DUBs, ubiquitin-specific proteases (USPs) subfamily is the largest and the most widely studied member. USP13, as an important deubiquitinase member belongs to USPs subfamilies, has been revealed as a potential therapeutic target for its significant role in tumor progression. *USP13* gene is amplified in human lung cancer and clinical samples of non-small cell lung cancer (NSCLC) showed tumor exhibited high USP13 level compared with adjacent normal tissues (17). Accordingly, USP13 depletion attenuated cell proliferation in NSCLC. Moreover, a recent study has shown USP13 was an important target of intrinsic insensitivity to afatinib in EGFR-mutant NSCLC. Genetic or pharmacological inhibition of USP13 could sensitize EGFR-mutant NSCLC to EGFR inhibition (18). Although USP13 plays vital role in tumor progression and drug resistance in NSCLC, its precisely biological functions and the regulatory mechanisms in SCLC remain undiscovered.

CSCs are highly reliant on elevated lipogenesis, which is reflected by the upregulation of master enzymes of lipogenesis, such as fatty acid synthase (FASN), ATP-citrate lyase (ACLY) and several fatty acid desaturases, including SCD1 and fatty acid desaturase 1 and 2 (FADS1 and FADS2) (19–22). Previous studies have reported that disorder of lipid metabolism or overactivated lipogenesis pathways are associated with tumor progression and treatment options in SCLC (23, 24). Pharmacological inhibition of lipogenic pathway significantly decreased viability of SCLC cell lines (25). Therefore, targeting lipid metabolism is regarded as a novel strategy against tumor cells, or even CSCs in SCLC.

In this present report, we determined to investigate the contribution of USP13 to SCLC progression. We found ectopic expression of USP13 promotes SCLC stemness and lipogenesis in a FASN-dependent manner, which provides a druggable vulnerability for SCLC patients.

MATERIALS AND METHODS

Cell Lines and Cell Culture Conditions

The human small cell lung cancer cell lines NCI-H1048 and NCI-H69, the multidrug-resistant cell line NCI-H69AR, and the human embryonic kidney cell line HEK-293T were purchased from ATCC. H446, H69 and H69AR cells were cultured in RPMI 1640 medium supplemented with 10% fetal bovine serum (FBS, Corning). H1048 cells were cultured in DMEM:F12 (Gibco) supplemented with 10% FBS, 0.005 mg/ml insulin (Sigma), 0.01 mg/ml transferrin (Gibco), 30 nM sodium selenite (Sigma), 10 nM hydrocortisone (Sigma), 10 nM beta-estradiol (Sigma) and 4.5 mM L-glutamine (Gibco). HEK-293T cells were cultured in DMEM (Gibco) supplemented with 10% FBS. Penicillin-streptomycin solution (10,000 U/mL) (Gibco) was added to the prepared culture medium with a 1:100 dilution. Cells were cultured in a humidified incubator at 37°C with 5% CO₂.

Lentivirus Packaging and Stable Cell Line Construction

Short hairpin RNA (shRNA) and wild-type plasmids were constructed by SyngenTech company (Beijing). Then, HEK-293T cells were transfected with the recombinant plasmids and packaging plasmids (pLP1, pLP2 and pLP/VSVG; Thermo Fisher Scientific) using Lipofectamine 3000 according to the instructions (Thermo). Forty-eight hours later, lentivirus particles were collected and stored at -80°C. The shRNA sequences used for knockdown were as follows: USP13-shRNA-1 5'-TGATTGAGATGGAGAATAA-3'; USP13-shRNA-2 5'-GCACGAAACTGAAGCCAAT-3'; FASN-shRNA 5'-CCTACTGGATGCGTTCTTCAA-3'.

For stable cell line construction, cells were infected with lentivirus in culture medium supplemented with 5 µg/ml polybrene (Sigma) for 24 hours. The effectively transfected cells were selected with the corresponding antibiotics. The gene expression efficiency was determined by immunoblot analyses.

RNA Extraction and Quantitative RT-PCR Analysis

Total RNA was extracted using RNA-Quick Purification Kit (ES-RN001, YISHAN Biotechnology) according to the manufacturer's protocol. Purified RNA was used to generate cDNA with TransScript All-in-One First-Strand cDNA Synthesis SuperMix (TransGen Biotech, AT341-01). qRT-PCR was performed with PerfectStart Green qPCR SuperMix (TransGen Biotech, AQ601-01) on an ABI 7900HT Real-Time PCR Thermocycler (Life Technologies). Relative mRNA expression was determined using the 2^{-ΔΔCt} method, and *actin* was used as an endogenous reference. The following primers

were used: *FASN* forward 5'-CAACTCACGCTCCGGAAA-3', reverse 5'-TGTGGATGCTGTCAAGGG-3'; *actin* forward 5'-ATCAAGATCATTGCTCCTCCTGAG-3', reverse 5'-CTGCTTGCTGATCCACATCTG-3'.

Immunoblotting and Immunoprecipitation Assays

Cells were lysed in RIPA buffer (89901, Thermo) containing proteinase and phosphatase inhibitor cocktail (78442, Thermo). Then, the cell lysates were quantified with a BCA protein assay kit (Thermo) according to the manufacturer's protocol. Equal amounts of protein from cell lysates were separated by SDS-PAGE and performed immunoblotting according previous description (26).

Cells were lysed in IP lysis buffer (87787, Thermo) containing proteinase and phosphatase inhibitor cocktail and rotated at 4 °C for 30 min. After centrifugation, the cell lysates were incubated overnight with indicated antibodies or normal IgG at 4 °C with rotary agitation. Protein A/G agarose beads (sc-2003, Santa Cruz Biotechnology) were added to the lysates and incubated for an additional 3 hours at 4 °C. Beads were washed three times with IP lysis buffer and boiled for 10 min in 1.5% SDS buffer. Whole cell lysates and immunoprecipitates were analyzed by immunoblot assay.

Antibodies that recognize USP13 (ab99421, 1:1000 dilution), Nanog (ab109250, 1:1000 dilution) and Oct4 (ab19857, 1:1000 dilution) were purchased from Abcam. Antibodies against *FASN* (3180, 1:1000 dilution), HA (3726, 1:1000 dilution), ubiquitin (3933, 1:1000 dilution) and CD133 (64326, 1:1000 dilution) were purchased from CST. Antibody against β -actin (A1978, 1:5000 dilution) was purchased from Sigma. Normal rabbit IgG (2729, 1:5000 dilution) and secondary antibodies, including anti-rabbit IgG HRP-linked antibody (7074, 1:3000 dilution) and anti-mouse IgG HRP-linked antibody (7076, 1:3000 dilution), were purchased from CST.

Protein Half-Life Detection

For the *FASN* protein half-life determination, H1048 cells expressing specific plasmids were treated with 100 μ g/ml cycloheximide (CHX, HY-12320, MedChem Express) for different periods of time. The cells were collected, and immunoblot analyses were performed with an anti-*FASN* antibody.

Immunofluorescence Analysis

H1048 cells were cultured on coverslips and then fixed in 4% paraformaldehyde for 20 min, followed by permeabilization with 0.1% Triton X-100 (in PBS) for 5 min. After washing with PBS, cells were blocked with 5% BSA for 1 hour at room temperature. Cells were then incubated with the indicated primary antibodies at 4°C overnight. After washing with PBS three times, the cells were incubated with secondary antibodies for 1 hour at room temperature and stained with DAPI (Invitrogen) by using ProLong™ Gold Antifade Mountant with DAPI (P36935, Invitrogen). The immunofluorescent staining was observed using a confocal microscope (Olympus).

Antibody that recognizes USP13 (sc-48357, 1:200) was purchased from Santa Cruz Biotechnology. Antibody against *FASN* (3180, 1:200) was purchased from CST. Anti-mouse IgG

(H+L) F(ab')₂ Fragment (Alexa Fluor 488 Conjugate) (4408, 1:1000 dilution) and anti-rabbit IgG (H+L) F(ab')₂ Fragment (Alexa Fluor 555 Conjugate) (4413, 1:1000 dilution) were purchased from CST.

LC-MS/MS Analysis

USP13 was immunoprecipitated from H1048 cells and separated by SDS-PAGE gel. Proteins in-gel were digested overnight in 12.5 ng/ μ l trypsin in 25 mM NH₄HCO₃. The peptides were extracted three times with 60% ACN/0.1% TFA and dried completely in a vacuum centrifuge. LC-MS/MS analysis was performed on a Q Exactive mass spectrometer (Thermo Scientific) coupled to an Easy nLC instrument (Thermo Fisher Scientific) for 60 min.

MS analysis was performed using the MASCOT engine (Matrix Science, London, UK; version 2.2) embedded in Proteome Discoverer 1.4 (Thermo Electron, San Jose, CA.) against the UniProt Human database and the decoy database. MS data were searched against the UniProt database (<https://www.uniprot.org/>). The cutoff of the global false discovery rate (FDR) for peptide and protein identification was set to 0.01. LC-MS/MS was performed by Shanghai Applied Protein Technology Co., Ltd (Shanghai, China).

Extreme Limiting Dilution Assay (ELDA)

H1048 or H69 cells were seeded into 96-well ultralow attachment plates (Corning) in DMEM/F12 (Gibco) supplemented with B27 (Gibco), 20 ng/mL epidermal growth factor (Gibco), and 20 ng/mL basic fibroblast growth factor (PeproTech) according previous description (27). After 7 days, the number of positive (sphere formation) wells in each group were uploaded and calculated in the ELDA website (28). The images were observed using an inverted fluorescence microscope (Olympus).

Measurement of Cellular Cholesterol and Triglyceride Levels

The indicated cells were seeded in 6 cm plates and incubated at 37°C with 5% CO₂ in an incubator. Until appropriate confluence, cellular cholesterol and triglyceride levels were extracted and determined using Cholesterol Quantitation Kit (MAK043, Sigma) and Triglyceride Quantification Kit (MAK266, Sigma) according to the manufacturer's protocol, respectively. Cholesterol and triglyceride levels were normalized to the protein concentration.

CD133⁺ Cells Sorting

H1048 or H69 cells were digested and separated into a single-cell suspension with PBS, then adjusted to a density of 1 \times 10⁷ cells/ml, and subsequently incubated with APC-conjugated anti-CD133 antibody (1:100 dilution) (397906, Biolegend) on ice for 30 min in the dark. Following two washes with PBS, cells were resuspended in 500 μ l PBS and subjected to isolation by flow cytometry (BD, LSRII). Negative control was determined by using equal amounts of APC-conjugated immunoglobulin G (IgG) (M1310G05, Biolegend)-stained cells.

Animal Studies

BALB/c nude mice (4–6 weeks old, female, 14–16 g) were purchased from Beijing HFK Bioscience Co. Ltd. and housed under specific

pathogen-free and controlled conditions (25–27, 45–55% humidity, 12 h day/night cycle). The study was approved by the Institutional Animal Care and Use Committee (IACUC) of the National Cancer Center/National Clinical Research Center for Cancer/Cancer Hospital, Chinese Academy of Medical Sciences and Peking Union Medical College, and the methods were carried out in accordance with the approved guidelines.

The cells were subcutaneously injected into the flanks of mice to establish a xenograft tumor. When the size of tumors reached approximately 100 mm³, animals were randomly divided into four groups and intraperitoneally injected with 10 mg/kg etoposide (S1225, Selleckchem), or 8 mg/kg TVB-2640 (#S9714, Selleckchem), or etoposide (10 mg/kg) and TVB-2640 (8 mg/kg) combination, or 0.9% saline as control. Tumor length (a) and minor diameter (b) were monitored once a week, and tumor size was calculated using the following formula: volume = $a \times b^2 / 2$.

Patients and Tissue Samples

SCLC samples with paired normal lung tissues were collected from patients who underwent radical resections at the Cancer Hospital of the Chinese Academy of Medical Sciences (Beijing, China) from January 2011 to January 2015. Surgically resected tissues have been pathologically diagnosed and stained with Mayer's hematoxylin and eosin (HE). After embedding into paraffin, tissue microarray (TMA) was then prepared by Superbiotek, Inc. Ethics approval was granted by the Committee for the Ethics Review of Research Involving Human Subjects of the Cancer Hospital of the Chinese Academy of Medical Sciences. **Table 1** summarized the clinical features of the patients.

Immunohistochemical (IHC) Analysis

Immunohistochemistry analyses were performed as previously described (29). Briefly, the human SCLC TMA slide was deparaffinized, rehydrated, autoclaved in 10 mM sodium citrate (pH 6.0) for 30 min to unmask antigens, and then incubated with primary antibodies against USP13 (ab99421, 1:200, Abcam), FASN (3180, 1:200, CST), Nanog (ab109250, 1:100, Abcam), or Oct4 (2750, 1:200, CST) at 4°C overnight. The slides were then incubated with secondary antibody, followed by chromogen diaminobenzidine (DAB) staining for signal amplification and detection. The IHC scores were assessed by two independent authors blinded to the treatment groups. IHC scoring was based on the percentage of positive cells and the staining intensity, as previously described (30).

Oil-Red O Staining

Oil Red O staining was performed on cryosections (6–10 μm) in thickness. In brief, the slides were fixed with formaldehyde, washed with 60% propylene glycerol, and then stained with 0.5% Oil Red O (Sangon Bio) in propylene glycerol for 10 min at 60°C. After staining, the slides were rinsed, counterstained with hematoxylin and mounted in glycerin. The red lipid droplets were visualized by microscopy.

Public Dataset

Public dataset GSE60052 were downloaded from the Gene Expression Omnibus (GEO, <https://www.ncbi.nlm.nih.gov/geo/>) database.

Statistical Analysis

Statistical analyses were conducted with a two-tailed unpaired Student's t test. Each experiment was carried out in at least triplicate, and all data are expressed as the mean ± SD. Kaplan–Meier analysis and log-rank tests were applied for survival analysis (31). The correlation between USP13 and FASN levels was analyzed using a Pearson correlation coefficient. *P* values < 0.05 were considered to be significant. Differences that are statistically significant are labeled with *(*p* < 0.05), **(*p* < 0.01), or ***(*p* < 0.001). Statistical analyses were performed by using GraphPad Prism (Version 9).

RESULTS

USP13 Is Overexpressed in SCLC and Predicts Poor Clinical Outcomes of SCLC Patients

To identify the important role of deubiquitinase USP13 in the clinical features of SCLC, we analyzed the mRNA expression of *USP13* in the published profile GSE60052. Overall survival analysis of *USP13* in SCLC patients showed that *USP13* was prognostically detrimental (**Figure 1A**), which indicated further necessary research of USP13. We then collected tumor tissues and the paired peripheral normal lung tissues which were surgically resected from patients diagnosed with SCLC. Immunohistochemical (IHC) analyses revealed that the expression of the USP13 protein was increased in SCLC tissues compared with normal lung tissues (**Figures 1B, C**). Next, we found that USP13 was significantly upregulated in the tissues of SCLC patients with lymph node metastasis (**Figure 1D**). Moreover, compared to patients evaluated as stage I, patients in stage II or stage III overexpressed USP13 (**Figure 1E**). Consistent with the previous analysis, Kaplan–Meier survival analysis demonstrated that high USP13 levels were correlated with poor overall survival of SCLC patients (**Figure 1F**). Collectively, these results demonstrated that USP13 is overexpressed in SCLC and predicts poor clinical outcomes.

Catalytically Active USP13 Promotes SCLC CSC-like Properties and Tumor Growth

As CSCs contribute to tumorigenesis, we examined the role of USP13 in SCLC stemness maintenance. The expression of stemness-related factors Oct4 and Nanog was dramatically decreased after depletion of USP13 with two different short hairpin RNAs (shRNAs) in H1048 and H69 cells (**Figure 2A**), which indicated an important role of USP13 in stemness maintenance. Consistently, silencing USP13 significantly inhibited sphere formation ability (**Figure 2B, Supplementary Figure 1A**). Conversely, forced expression of WT USP13 but not the catalytically inactive USP13 (C345A) mutant significantly promoted Oct4 and Nanog expression (**Figure 2C**) and sphere formation ability (**Figure 2D, Supplementary Figure 1B**). CD133⁺ cells are widely considered to be SCLC stem-like cells (32). To validate the expression levels of USP13 in SCLC CSCs, we

TABLE 1 | Clinical characteristics of 90 SCLC patients.

Characteristics		Total (cases)	Percentage (%)
Age (years)	≤ 60	57	63%
	> 60	33	37%
Gender	Male	75	83%
	Female	15	17%
Smoking status	Non-smoker	22	24%
	smoker	68	76%
Vascular invasion	No	15	17%
	Yes	21	23%
	Unknown	54	60%
Lymph Node Metastasis	No	26	≈29%
	Yes	64	≈71%
TNM stage	I	24	≈27%
	II	47	≈52%
	III	19	≈21%

enriched CD133⁺ subpopulations from H1048 cells with an anti-CD133 antibody. As shown in **Figure 2E** and **Supplementary Figure 1C**, USP13 expression level in CD133⁺ subpopulation was substantially higher than that in the CD133⁻ subpopulation. Together, these results support a critical role of USP13 which depends on its catalytic function in promoting SCLC stemness.

We next determined the role of USP13 in tumor growth by subcutaneously injecting H1048 cells with or without USP13 depletion, or USP13 depletion combined with WT USP13 or catalytically inactive USP13 (C345A) mutant overexpression (**Supplementary Figure 1D**) in mice. The results showed that mice inoculated with USP13-deficient cells evidently formed smaller tumor masses than those inoculated with control cells, and this reduction was abrogated by reconstituted expression of shRNA-resistant WT USP13 but not the catalytically inactive USP13 (C345A) mutant (**Figure 2F**). Moreover, IHC staining analysis in tumor tissues showed that Nanog and Oct4 expression decreased after USP13 depletion, and this decrease was rescued by reconstituted expression of WT USP13 but not catalytically inactive USP13 (C345A) mutant (**Figures 2G, H**). Hence, our data strongly indicated that USP13 promotes SCLC tumor growth.

USP13-Dependent FASN Expression Promotes SCLC Stemness and Lipogenesis

To verify mechanisms involved in USP13 regulated SCLC stemness, immunoprecipitation (IP) was performed with an anti-USP13 antibody and mass spectrometry (MS) were used to identify proteins that interacts with USP13. MS analysis revealed 2 unique peptides identical to FASN (**Supplementary Figure 2A**), which is a critical enzyme for the synthesis of palmitate (precursor of cholesterol and triglyceride) from acetyl-CoA and malonyl-CoA and contributes to CSC maintenance (33). We confirmed the interaction between endogenous USP13 and FASN by the co-

immunoprecipitation (Co-IP) of H1048 cell lysates (**Figure 3A**). Consistently, USP13 and FASN were shown to interact physically by immunofluorescence (IF) analyses (**Figure 3B**). To determine the importance of USP13 in the regulation of FASN, we then analyzed FASN expression with or without USP13 depletion or overexpression. As shown in **Figures 3C, D**, USP13 downregulation decreased (**Figure 3C**), whereas USP13 overexpression increased FASN protein levels (**Figure 3D**) without affecting FASN mRNA levels (**Supplementary Figure 2B**). To detect the role of USP13-FASN axis in regulating cancer stemness and lipogenesis in SCLC, we stably depleted FASN after WT USP13 reconstitution in USP13 knockdown cells. USP13 depletion in SCLC cells decreased the expression levels of Oct4 and Nanog (**Figure 3E**), reduced the sphere formation ability (**Figure 3F**) and cellular cholesterol and triglyceride levels (**Figure 3G**). In contrast, overexpression of reconstituted WT USP13 in SCLC increased Oct4 and Nanog expression (**Figure 3E**), promoted sphere formation ability (**Figure 3F**) and increased cellular cholesterol and triglyceride levels (**Figure 3G**). Importantly, the effects of USP13 on SCLC cancer stemness maintenance and lipogenesis were abrogated by FASN depletion (**Figures 3E–G**). In addition, IHC analysis and oil red O staining of tumor tissues indicated that USP13-dependent FASN expression increases lipogenesis (**Supplementary Figures 2C, D**). These results indicated USP13 promotes cancer stemness and lipogenesis mainly through FASN.

USP13 Inhibits Polyubiquitylation-Dependent FASN Degradation

As a deubiquitinase, we hypothesized that endogenous USP13 could regulate FASN stability. We treated USP13 knockdown cells with the proteasome inhibitor MG-132 and found that inhibition of FASN expression by USP13 depletion was clearly blocked by MG-132 treatment in H1048 and H69 cells (**Figure 4A**). To determine

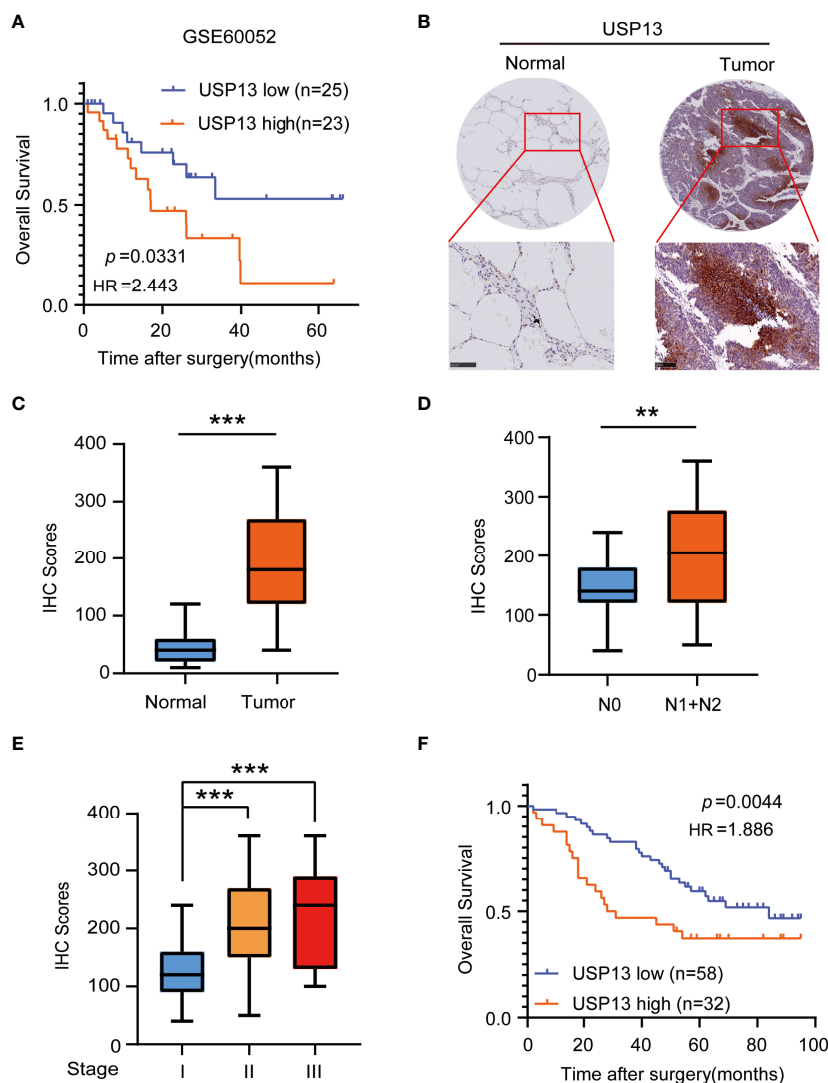


FIGURE 1 | USP13 is overexpressed in SCLC and predicts poor clinical outcomes. **(A)** Kaplan-Meier analysis of overall survival curves from a public dataset (GSE60052) for SCLC patients with low or high USP13 expression. p values are calculated using a log-rank test (two-tailed). **(B, C)** Immunohistochemical analysis of USP13 in SCLC tumor specimens (T) and their adjacent normal tissues (N). Representative IHC images are shown **(B)**. IHC scores of USP13 expression were calculated **(C)**. Scale bars: 500 μ m. Data represent the means \pm SD of samples. Two-tailed student's t -test was used. *** $p < 0.001$. **(D)** The expression of USP13 in SCLC patients with or without lymph node metastasis is shown. Data represent the means \pm SD of samples. Two-tailed student's t -test was used. ** $p < 0.01$. **(E)** USP13 expression levels are shown in SCLC patients of different cancer stages. Data represent the means \pm SD of samples. Two-tailed student's t -test was used. *** $p < 0.001$. **(F)** The Kaplan-Meier method with a two-tailed log-rank test was used to plot survival curves for SCLC patients with high and low USP13 expression.

whether USP13 stabilizes the FASN protein through deubiquitination, we first examined FASN protein turnover by using cycloheximide (CHX) and traced the protein levels. Indeed, the FASN protein was gradually degraded with CHX treatment. As anticipated, the FASN protein half-life was decreased after depletion of USP13 (**Figure 4B**), while ectopic WT USP13 but not catalytically inactive USP13 (C345A) mutant expression largely increased FASN stability (**Figure 4C**). Moreover, we found that depletion of USP13 enhanced the ubiquitination level of endogenous FASN (**Figure 4D**). In contrast, forced expression of

WT USP13 but not the catalytically inactive USP13 (C345A) mutant reduced the ubiquitination of FASN (**Figure 4E**). Overall, our experiments indicate that USP13 promotes FASN protein stability by decreasing polyubiquitination of FASN and thus prevents its degradation through the proteasome pathway.

FASN is Positively Correlates with USP13

To determine the clinical significance of FASN expression, we performed IHC analyses of SCLC tissue specimens. IHC staining

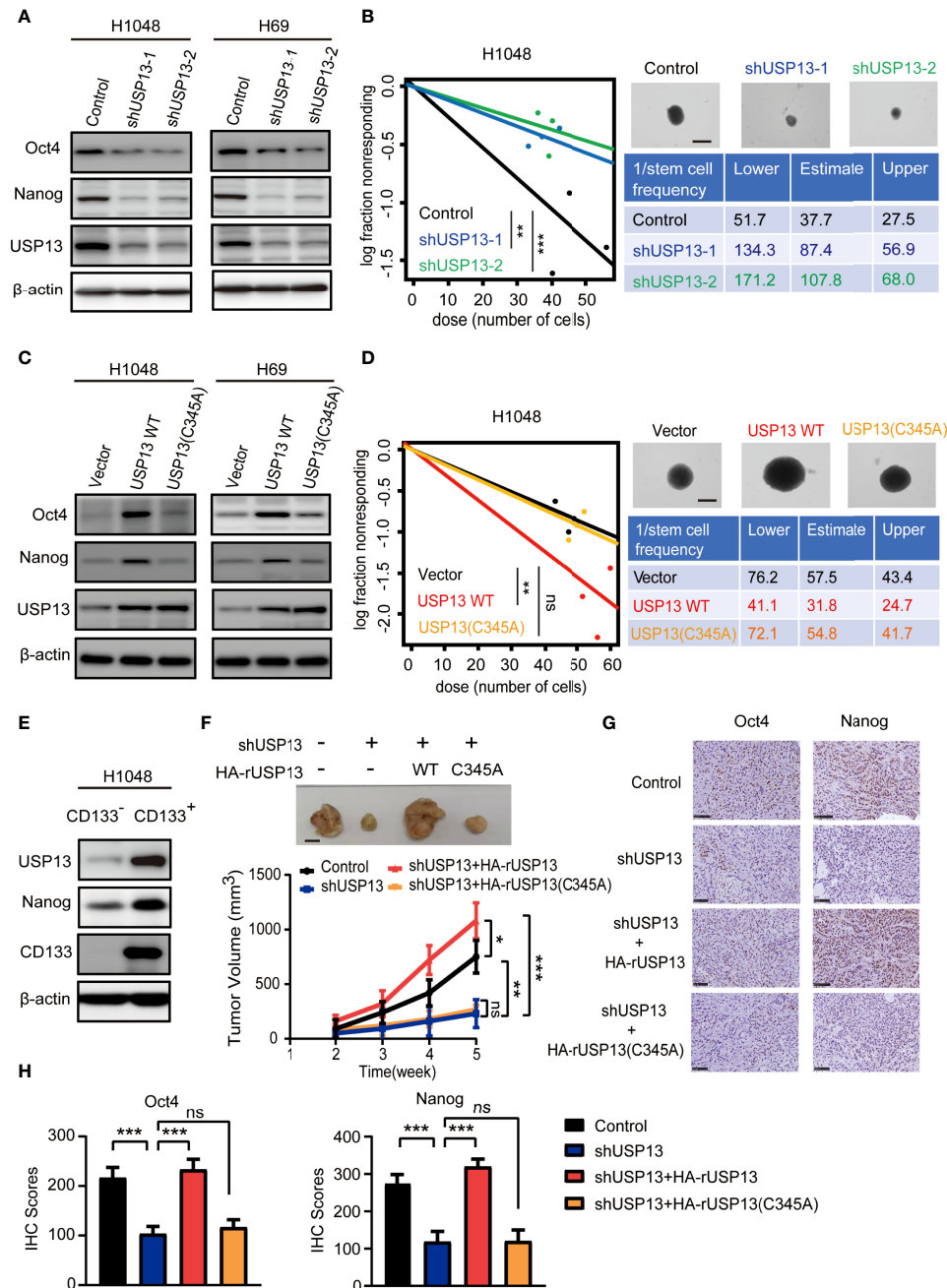


FIGURE 2 | USP13 promotes SCLC CSC-like properties and tumor growth. **(A)** Immunoblot analyses of H1048 (left) and H69 (right) cells with or without USP13 depletion were performed with the indicated antibodies. **(B)** Left: ELDA was performed in H1048 cells with or without USP13 knockdown. Representative sphere images (top right) and stemness frequency illustration of the cells with the upper and lower 95% confidence intervals (bottom right) are shown. Scale bars, 50 μ m. Data represent the means \pm SD of wells. Two-tailed student's t-test was used. $**p < 0.01$, $***p < 0.001$. **(C)** Immunoblot analyses of H1048 (left) and H69 (right) cells with or without WT USP13 or catalytically inactive USP13 (C345A) mutant overexpression were performed with the indicated antibodies. **(D)** Left: ELDA was performed in H1048 cells with or without WT USP13 or catalytically inactive USP13 (C345A) mutant overexpression. Representative sphere images (top right) and stemness frequency illustration of the cells with the upper and lower 95% confidence intervals (bottom right) are shown. Scale bars, 50 μ m. Data represent the means \pm SD of wells. Two-tailed student's t-test was used. ns, not significant. $**p < 0.01$. **(E)** CD133⁻ and CD133⁺ subpopulations of H1048 cells were sorted. Immunoblot analyses were performed with the indicated antibodies. **(F)** Tumor formation in immunodeficient mice transplanted with H1048 cells with or without USP13 depletion, or shUSP13 cells combined with reconstituted expression of WT HA-rUSP13 or catalytically inactive HA-rUSP13 (C345A) mutant. Tumor sizes and volumes were measured and calculated (n=5 per group). Data represent the means \pm SD of five mice per group. Two-tailed student's t-test was used. ns, not significant. $*p < 0.05$, $**p < 0.01$, $***p < 0.001$. **(G, H)** IHC staining of mouse tumor tissues was performed with the indicated antibodies. Representative images are displayed **(G)**, and IHC scores were calculated **(H)**. Scale bars: 100 μ m. Data represent the means \pm SD of triplicate samples. Two-tailed student's t-test was used. ns, not significant. $***p < 0.001$.

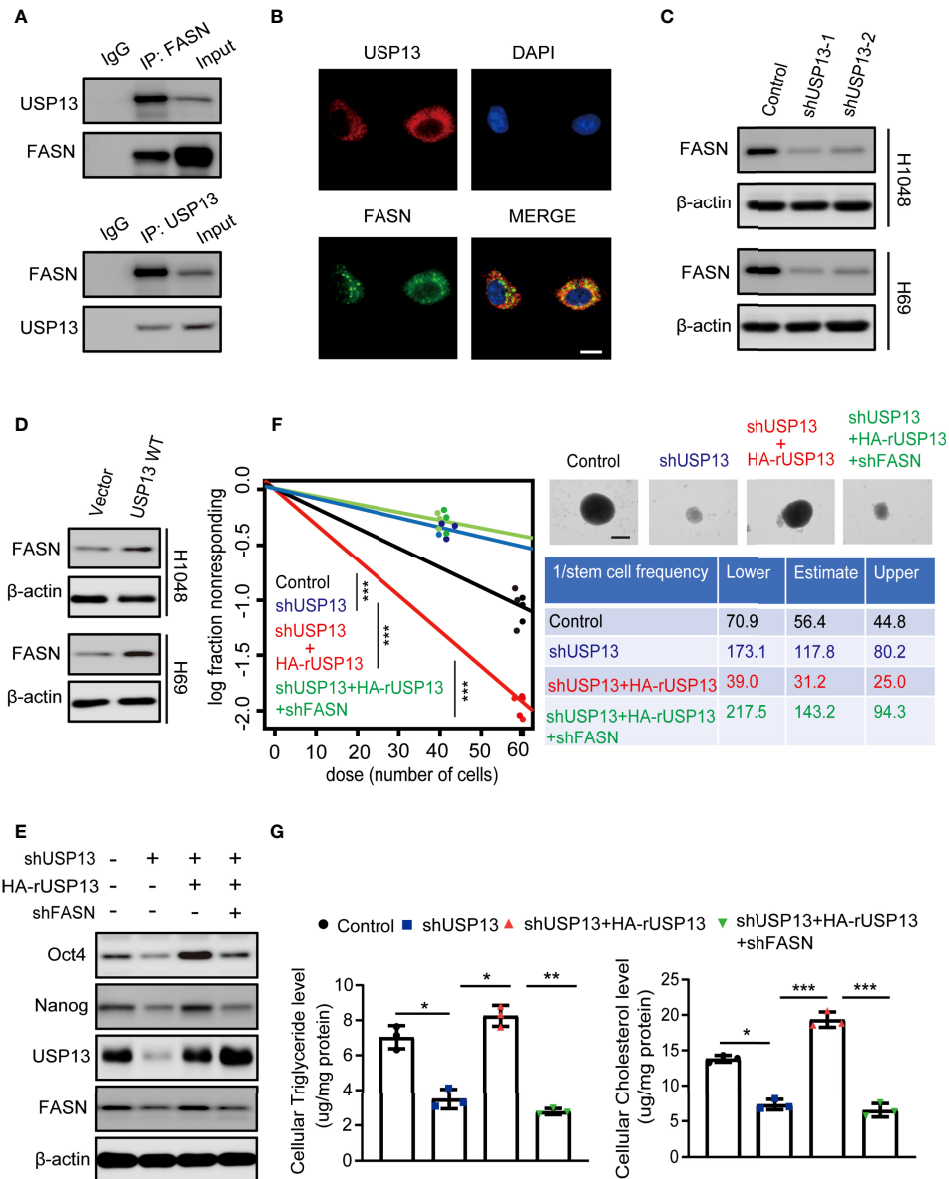


FIGURE 3 | USP13-dependent FASN expression promotes SCLC stemness and lipogenesis. **(A)** Immunoprecipitation and immunoblot analyses were performed with the indicated antibodies in H1048 cells. **(B)** Immunofluorescence analyses were performed with the indicated antibodies in H1048 cells. DAPI was used for nuclear staining. Scale bars: 20 μ m. **(C, D)** FASN expression levels were detected in H1048 (top) or H69 (bottom) cells with or without USP13 depletion **(C)** or overexpression **(D)** by immunoblot analyses with an anti-FASN antibody. **(E)** H1048 cells with or without USP13 shRNA expression, or USP13 depletion reconstituted expression of WT HA-rUSP13 with or without FASN depletion were analyzed by immunoblotting with the indicated antibodies. **(F)** Left: ELDA was performed in H1048 cells with or without USP13 shRNA expression, or USP13 depletion combined with reconstituted expression of WT HA-rUSP13 with or without FASN depletion. Representative sphere images (top right) and stemness frequency illustration of the cells with the upper and lower 95% confidence intervals (bottom right) are shown. Scale bars, 50 μ m. Data represent the means \pm SD of wells. Two-tailed student's t-test was used. *** p < 0.001. **(G)** Cellular triglyceride levels (left) and cholesterol levels (right) in H1048 cells with or without USP13 shRNA expression, or USP13 depletion combined expression of reconstituted expression of WT HA-rUSP13 with or without FASN depletion were determined. Data shown are the mean \pm S.D. ($n=3$). Two-tailed student's t-test was used. * p < 0.05, ** p < 0.01, *** p < 0.001.

showed FASN was highly upregulated in SCLC tissues than in the paired adjacent normal tissues (**Figures 5A, B**). More importantly, the expression of FASN was stage-dependent (**Figure 5C**). In addition, patients with high FASN expression had shorter survival duration than those with low FASN

expression (**Figure 5D**). Consistent with previous results, FASN protein expression levels were positively correlated with USP13 expression levels (**Figure 5E**). These results strongly suggested that USP13-stabilized FASN expression promotes clinical aggressiveness of SCLC.

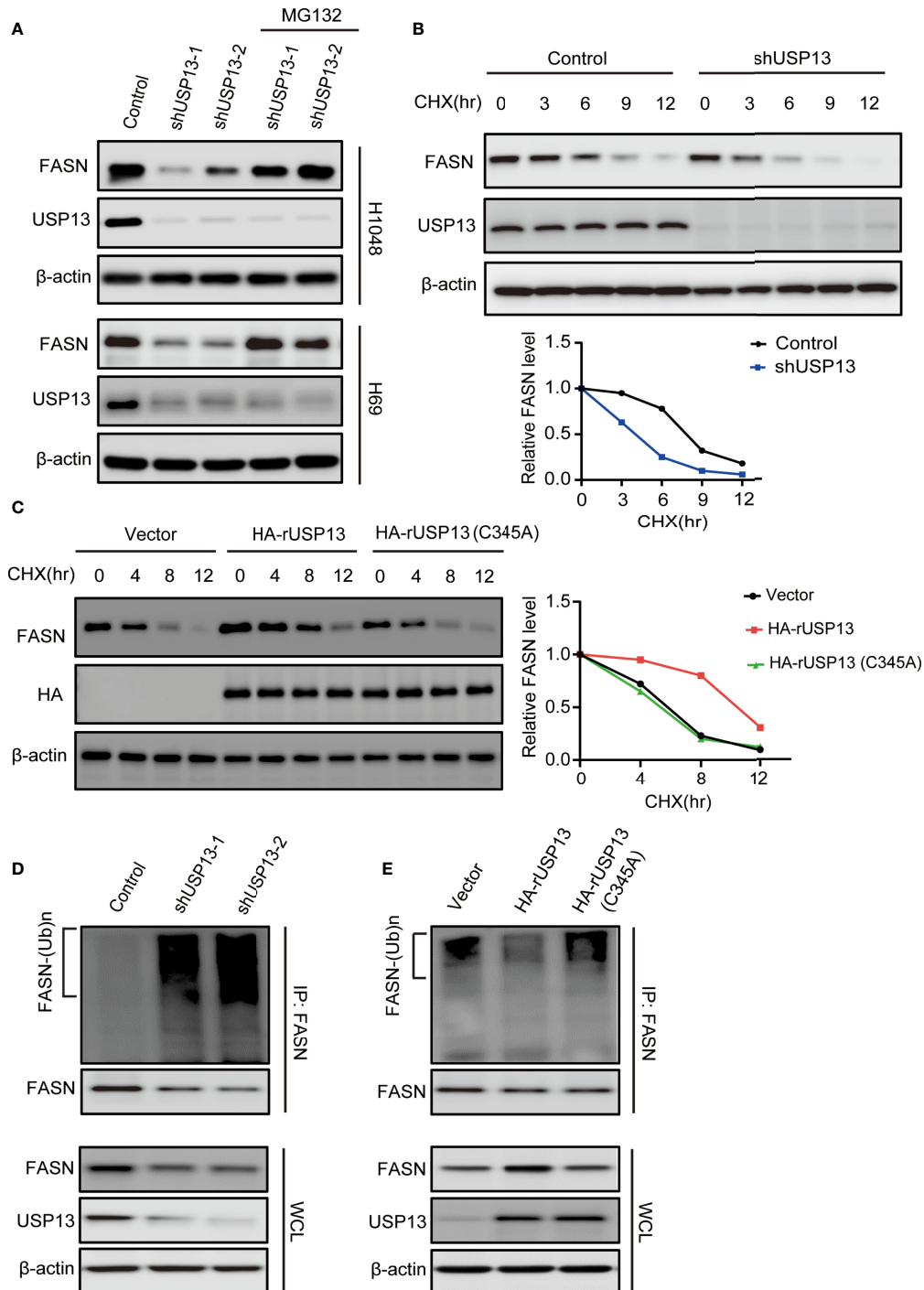


FIGURE 4 | USP13 inhibits polyubiquitylation-dependent FASN degradation. **(A)** H1048 (upper) and H69 (lower) cells expressing two different USP13 shRNAs were treated with MG132 (50 μ M) for 8 hours. Immunoblot analyses were performed with the indicated antibodies. **(B)** H1048 cells with or without USP13 depletion were treated with CHX (100 μ g/ml) for the indicated periods of time. FASN expression levels were analyzed with an anti-FASN antibody (upper) and quantification of FASN levels relative to β -actin expression levels (lower) were performed. **(C)** H1048 cells with or without WT USP13 or catalytically inactive USP13 (C345A) mutant overexpression were treated with CHX (100 μ g/ml) for the indicated periods of time. Immunoblot analyses were performed with the indicated antibodies (left). Quantification of FASN expression levels relative to β -actin expression levels is shown (right). **(D)** H1048 cells expressing two different USP13 shRNAs or a control shRNA were treated with MG132 (50 μ M) for 8 hours. Immunoprecipitation and immunoblot analyses were performed with the indicated antibodies. **(E)** H1048 cells with or without WT USP13 or catalytically inactive USP13 (C345A) mutant overexpression were treated with MG132 (50 μ M) for 8 hours. Immunoprecipitation and immunoblot analyses were performed with the indicated antibodies.

FASN Inhibition Attenuates SCLC Lipogenesis, Self-Renewal Properties, Chemotherapy Resistance and USP13-Dependent Tumorigenesis

Since FASN is a key enzyme involved in USP13-promoted cancer stemness, we further examined whether FASN inhibitor could be a favorable treatment strategy. TVB-2640, a highly potent and

selective FASN inhibitor, was designed to reduce hepatic fat in nonalcoholic fatty liver disease (NAFLD) and nonalcoholic steatohepatitis (34, 35). More importantly, with compelling support as an oncology therapeutic drug, TVB-2640 was the first highly selective FASN inhibitor to enter clinical studies (36). We found that TVB-2640 treatment decreased cellular cholesterol and triglyceride levels and reduced sphere

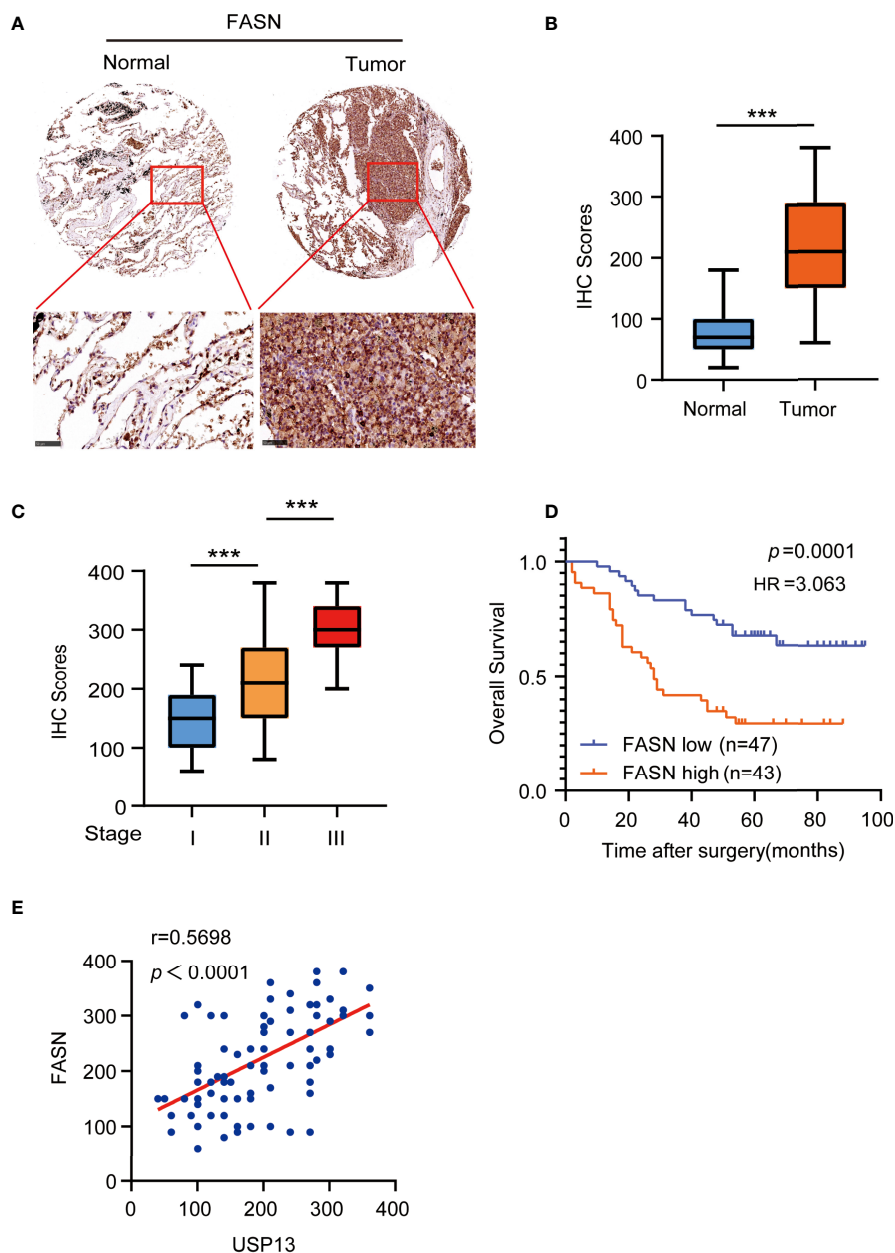


FIGURE 5 | FASN is positively correlates with USP13. **(A, B)** Representative images **(A)** of IHC staining for FASN protein on tissue microarray (TMA) composed of SCLC tumor specimens (T) with their adjacent normal tissues (N). IHC score **(B)** was calculated. Scale bars: 100 μ m. Data represent the means \pm SD of samples. Two-tailed student's t-test was used. *** $p < 0.001$. **(C)** FASN expression levels are shown in SCLC patients of different cancer stages. Data represent the means \pm SD of samples. Two-tailed student's t-test was used. *** $p < 0.001$. **(D)** Kaplan-Meier plots of the overall survival time of 90 SCLC patients with low or high expression levels of FASN. p values are calculated using a log-rank test (two-tailed). **(E)** The correlation between USP13 and FASN expression in an SCLC tissue microarray was analyzed using a two-tailed Pearson correlation coefficient.

formation ability in a dose- and time-dependent manner in both H1048 and H69 cells (**Figures 6A–D, Supplementary Figures 3A, B**). Given that FASN expression is associated with chemoresistance (37), targeting lipid metabolism might be a new potential therapy for SCLC patients with acquired drug-resistance. We subcutaneously injected multi-drugs resistant H69AR cells into mice (38), then treated with VP16 (etoposide) or TVB-2640 for monotherapy, or concurrent therapy with VP16 and TVB-2640. Consistent with previous study (38), tumors in the VP16 treatment group displayed slight shrinkage (**Figure 6E**). Importantly, TVB-2640 treatment dramatically suppressed tumor growth (**Figure 6E**). In addition, the group treated with both VP16 and TVB-2640 showed an improved better response than the group treated with TVB-2640 alone (**Figure 6E**), indicated synergistic treatment effect. IHC staining analysis confirmed that lipogenesis inhibition by TVB-2640 repressed SCLC stemness features, reflected by decreased Nanog expression, and in combination with classical chemotherapeutics induced a dramatic synergistic effect (**Supplementary Figure 3C**). To further study whether TVB-2640 treatment can reverse USP13-mediated tumor formation, we subcutaneously injected H1048 cells with or without USP13 depletion, or H1048 USP13-depleted cells with reconstituted expression of shRNA-resistant WT USP13 with or without TVB-2640 treatment. Consistent with previous result, USP13 depletion dramatically suppressed tumor growth, and forced overexpression of WT HA-rUSP13 rescued the decreased tumor volume (**Figure 6F**). Importantly, TVB-2640 treatment can significantly reduce the tumorigenesis caused by USP13 overexpression. Together, these data show that the FASN inhibitor TVB-2640 can be used as a potential chemotherapy combination anti-SCLC drug.

DISCUSSION

The molecular function of USP13 in tumorigenesis has been controversial in different cancers according to previous studies. USP13 was first found to deubiquitinate tumor suppressor protein PTEN in human breast cancer cells, which indicated a tumor-suppressing role for USP13 (39). However, further studies revealed that USP13 may have context-dependent functions in cancer development by interacting with different substrates to regulate protein stability. *USP13* gene is amplified in serious ovarian cancers and specifically deubiquitinates and thus upregulates two key metabolic key enzymes, ATP citrate lyase (ACLY) and oxoglutarate dehydrogenase (OGDH). As a consequence, USP13 overexpression is correlated with poor clinical outcome (40). In lung and ovarian cancer cells, USP13 deubiquitinates and stabilizes MCL1, a key member of the anti-apoptotic BCL-2 family. Pharmacological inhibition of USP13 with spautin-1 significantly inhibits tumor growth and increases tumor cell sensitivity to BH3 mimetic inhibitors, which suggests that targeting USP13 may be a valuable strategy for cancer

treatment (41). As a highly expressed protein in glioma stem cells (GSCs), USP13 maintains GSC self-renewal abilities by stabilizing the critical transcription factor *c-Myc* (42). Consistently, we found that USP13 plays an oncogenic role to maintain SCLC stemness and tumorigenic potential, which is dependent on its catalytic activity. Importantly, USP13 expression is positively correlated with cancer progression and predicts poor survival of SCLC patients. Further mechanistic studies revealed that USP13 interacts with and stabilizes FASN by reducing FASN polyubiquitination, suggesting a putative target for SCLC treatment.

Previous studies have shown that cancer cells reprogram lipogenic metabolism in response to the massive demand for macromolecules and bioenergy (43, 44), and that increased expression of FASN is a prominent feature (45). In KRAS signaling active lung adenocarcinomas, FASN is a primary responder that induces elevated lipogenesis which mediated by the ERK pathway. Inhibition of FASN by cerulenin blocked proliferation of KRAS-driven lung cancer cells, indicating a promising role of lipid metabolism in tumor treatment (46). Subsequent studies in EGFR mutated non-small cell lung cancer confirmed that FASN-associated fatty acid metabolic pathway upregulation was the main principal for tyrosine kinase inhibitor (TKI)-resistant EGFR mutated NSCLC growth (47). In our studies, FASN was induced by the stemness-related deubiquitinase USP13 in SCLC, implying that lipogenesis can augment the self-renewal property, and that effectively inhibiting FASN activity may provide an alternative treatment. Although FASN inhibitors, including C75, C93, GSK837149A, Orlistat and TVB-3166, have demonstrated preclinical antitumor activity in cancer cell lines and xenograft models (45, 48), none of these compounds have been tested in cancer patients due to side effects. Therefore, we selected the FASN inhibitor TVB-2640, which has a favorable tolerability profile and entered a phase II clinical trial (36), as treatment strategy for SCLC. Our results showed that accompanied by decreased triglyceride and cholesterol levels, TVB-2640 significantly suppressed self-renewal ability of SCLC. Further *in vivo* animal studies revealed TVB-2640 sensitized chemotherapy-resistant tumor cells to etoposide treatment and inhibited USP13-dependent cancer stemness and tumor growth, suggesting a crucial role of lipogenic pathway in SCLC proliferation and drug resistance. Previous research has identified that MEK5/ERK5 dual kinase axis supporting SCLC survival heavily relies on the mevalonate pathway, which controls cholesterol synthesis (25). Corroborative evidence has shown that mutated FASN, which may affect dimer formation or enzyme activity, occurs in SCLC patients and indicates a better prognosis in those who have received chemotherapy (49). These results support that abnormal expression of proteins involved in lipogenic pathways synergistically promotes cancer cell survival, which provides a more efficacious strategy for treatment of SCLC. Finally, the clinical significance of FASN expression in our cohort was evidenced by its positive association with SCLC patient clinical stage and poor overall survival.

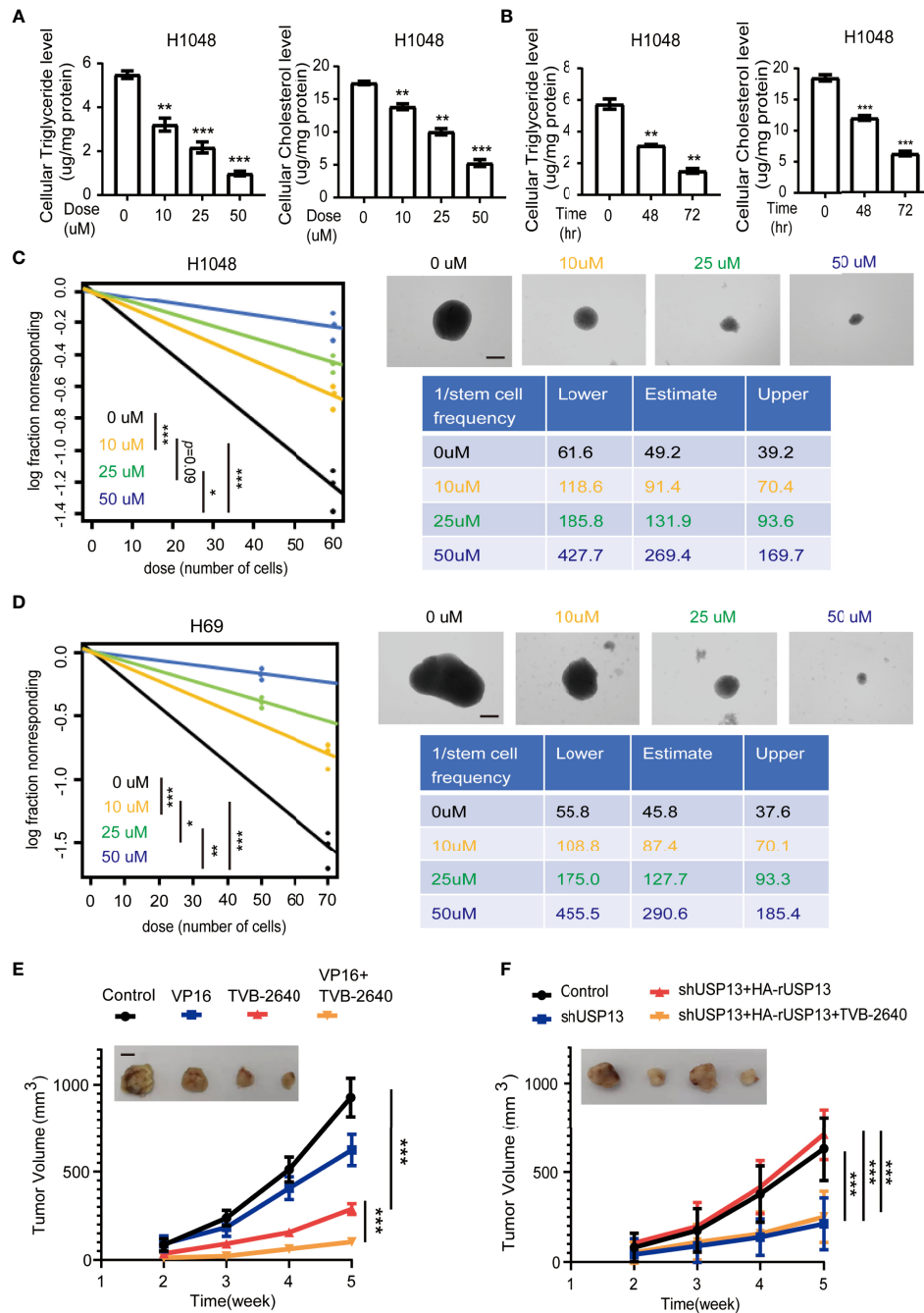


FIGURE 6 | FASN inhibition attenuates SCLC lipogenesis, self-renewal properties, chemotherapy resistance and USP13-dependent tumorigenesis. **(A)** Triglyceride (left) and cholesterol (right) levels were measured in H1048 cells treated with the FASN inhibitor TVB-2640 at the indicated doses for 72 hours. DMSO was used as the vehicle control. Data represent the means \pm SD of triplicate samples. Two-tailed student's t-test was used. $**p < 0.01$, $***p < 0.001$. **(B)** Triglyceride (left) and cholesterol (right) levels were measured in H1048 cells after 50 μ M FASN inhibitor TVB-2640 treatment for the indicated periods of time. Data represent the means \pm SD of triplicate samples. Two-tailed student's t-test was used. $*p < 0.01$, $***p < 0.001$. **(C, D)** Left: ELDA was performed in H1048 **(C)** and H69 **(D)** cells with or without FASN inhibitor TVB-2640 treatment at the indicated dose. Representative sphere images (top right) and stemness frequency illustration of the cells with the upper and lower 95% confidence intervals (bottom right) are shown. Scale bars, 50 μ m. Data represent the means \pm SD of wells. Two-tailed student's t-test was used. $*p < 0.05$, $**p < 0.01$, $***p < 0.001$. **(E)** Nude mice were subcutaneously injected with H69AR cells and intraperitoneally injected with indicated drugs when the size of the tumor reached approximately 100 mm^3 . Tumor sizes and volumes were measured and calculated ($n=5$ per group). Data represent the means \pm SD of five mice per group. Two-tailed student's t-test was used. $*p < 0.05$, $**p < 0.01$, $***p < 0.001$. **(F)** H1048 cells with or without USP13 depletion, or shUSP13 cells combined with reconstituted expression of WT HA-rUSP13 were subcutaneously injected into nude mice and then with or without TVB-2640 treatment. Tumor sizes and volumes were measured and calculated ($n=5$ per group). Data represent the means \pm SD of five mice per group. Two-tailed student's t-test was used. ns, not significant. $***p < 0.001$.

CONCLUSIONS

In this study, we showed that USP13 promotes SCLC stemness and lipogenesis by inhibiting proteasome-dependent FASN degradation. Pharmacological inhibition of FASN with the small molecule TVB-2640 impaired self-renewal and tumor growth ability of SCLC.

DATA AVAILABILITY STATEMENT

The datasets presented in this study can be found in online repositories. The names of the repository/repositories and accession number(s) can be found below: <http://proteomexchange.org/>, PXD032993.

ETHICS STATEMENT

The study was approved by the Institutional Animal Care and Use Committee (IACUC) of the National Cancer Center/National Clinical Research Center for Cancer/Cancer Hospital, Chinese Academy of Medical Sciences and Peking Union Medical College, and the methods were carried out in accordance with the approved guidelines. Written informed consent was obtained from the individual(s) for the publication of any potentially identifiable images or data included in this article.

AUTHOR CONTRIBUTIONS

YG and JW conceived and designed the study; JH provided critical scientific input. JW, WL, RL, HC, SS, FS, and YY performed the experiments. JH, XF, SG, and YG established the patient cohort and biobanking of specimen for tissue microarray. JW wrote the draft manuscript. YG revised the manuscript. All authors contributed to the article and approved the submitted version.

FUNDING

This work was supported by National Key R&D Program of China (2020AAA0109500, JH), National Natural Science Foundation of China (82122053, YG, 82188102, JH), the Beijing Municipal Science & Technology Commission (Z191100006619118, JH), R&D Program of Beijing Municipal Education commission (KJZD20191002302, JH), CAMS Initiative for Innovative Medicine (2021-1-I2M-012, JH, 2021-1-I2M-015, SG), Non-profit Central Research Institute Fund of

Chinese Academy of Medical Sciences (2021-PT310-001, YG), and Aiyou Foundation (KY201701, JH).

SUPPLEMENTARY MATERIAL

The Supplementary Material for this article can be found online at: <https://www.frontiersin.org/articles/10.3389/fonc.2022.899987/full#supplementary-material>

Supplemental Figure 1 | USP13 promotes SCLC CSC-like properties:

(A) Left: ELDA was performed in H69 cells with or without USP13 knockdown. Representative sphere images (top right) and stemness frequency illustration of the cells with the upper and lower 95% confidence intervals (bottom right) are shown. Scale bars, 50 μ m. Data represent the means \pm SD of wells. Two-tailed student's t-test was used. *** $p < 0.001$. **(B)** Left: ELDA was performed in H69 cells with or without WT USP13 or catalytically inactive USP13 (C345A) mutant overexpression. Representative sphere images (top right) and stemness frequency illustration of the cells with the upper and lower 95% confidence intervals (bottom right) are shown. Scale bars, 50 μ m. Data represent the means \pm SD of wells. Two-tailed student's t-test was used. ns, not significant. *** $p < 0.001$. **(C)** CD133⁻ and CD133⁺ subpopulations of H69 cells were sorted. Representative cell fractions were separated by flow cytometry sorting (upper). Immunoblot analyses were performed with the indicated antibodies (lower). **(D)** Immunoblot analyses were performed in H1048 cells with or without USP13 depletion, or shUSP13 cells combined with reconstituted expression of WT HA-rUSP13 or catalytically inactive HA-rUSP13 (C345A) mutant the indicated antibodies.

Supplemental Figure 2 | USP13-dependent FASN expression promotes

SCLC stemness and lipogenesis: (A) H1048 cells were immunoprecipitated with anti-USP13 antibody and analyzed by mass spectrometry. The selected FASN peptide identified by mass spectrometry analyses was shown. **(B)** Relative mRNA level of FASN was detected in H1048 cells with or without USP13 depletion (top) or overexpression (bottom). Data shown are the mean \pm S.D. ($n=3$). ns, not significant. **(C, D)** IHC staining of FASN with anti-FASN antibody and the oil red O staining were performed by using tumor tissues as described in Figure 2F. Representative images are displayed **(C)**. IHC scores **(D, top right)** and oil red O-stained areas **(D, bottom right)** were calculated. Scale bars: 100 μ m. Data represent means \pm SD of triplicate samples. Two-tailed student's t-test was used. ns, not significant. * $p < 0.05$, ** $p < 0.01$, *** $p < 0.001$.

Supplemental Figure 3 | FASN inhibition attenuates SCLC lipogenesis:

(A) Triglyceride (left) and cholesterol (right) levels were measured in H69 cells based on FASN inhibitor TVB-2640 treatment with indicated dose for 72 hours. DMSO was used as control vehicle. Data represent means \pm SD of triplicate samples. Two-tailed student's t-test was used. ** $p < 0.01$, *** $p < 0.001$. **(B)** Triglyceride (left) and cholesterol (right) levels were measured in H69 cells after 50 μ M FASN inhibitor TVB-2640 treatment for the indicated periods of time. Data represent means \pm SD of triplicate samples. Two-tailed student's t-test was used. *** $p < 0.001$. **(C)** IHC staining of Nanog expression and the oil red O staining were performed with mouse tumor tissues. Representative images are displayed (left). IHC scores (top right) and oil red O-stained areas (bottom right) were calculated. Scale bars: 100 μ m. Data represent the means \pm SD of triplicate samples. Two-tailed student's t-test was used. ns, not significant. * $p < 0.05$, ** $p < 0.01$.

REFERENCES

- Byers LA, Rudin CM. Small Cell Lung Cancer: Where Do We Go From Here? *Cancer* (2015) 121:664–72. doi: 10.1002/cncr.29098
- Siegel RL, Miller KD, Jemal A. Cancer Statistics, 2020. *CA: Cancer J Clin* (2020) 70:7–30. doi: 10.3322/caac.21590
- Hu W, Wei H, Li K, Li P, Lin J, Feng R. Downregulation of USP32 Inhibits Cell Proliferation, Migration and Invasion in Human Small Cell Lung Cancer. *Cell Prolif* (2017) 50(4):e12343. doi: 10.1111/cpr.12343
- Coles GL, Cristea S, Webber JT, Levin RS, Moss SM, He A, et al. Unbiased Proteomic Profiling Uncovers a Targetable GNAS/PKA/PP2A Axis in Small Cell Lung Cancer Stem Cells. *Cancer Cell* (2020) 38:129–143.e127. doi: 10.1016/j.ccell.2020.05.003
- Byers LA, Wang J, Nilsson MB, Fujimoto J, Saintigny P, Yordy J, et al. Proteomic Profiling Identifies Dysregulated Pathways in Small Cell Lung Cancer and Novel Therapeutic Targets Including PARP1. *Cancer Discovery* (2012) 2:798–811. doi: 10.1158/2159-8290.CD-12-0112
- Cardnell RJ, Feng Y, Diao L, Fan YH, Masrorpour F, Wang J, et al. Proteomic Markers of DNA Repair and PI3K Pathway Activation Predict Response to

- the PARP Inhibitor BMN 673 in Small Cell Lung Cancer. *Clin Cancer Res* (2013) 19:6322–8. doi: 10.1158/1078-0432.CCR-13-1975
7. Yu J, Wang S, Zhao W, Duan J, Wang Z, Chen H, et al. Mechanistic Exploration of Cancer Stem Cell Marker Voltage-Dependent Calcium Channel $\alpha_2\delta_1$ Subunit-Mediated Chemotherapy Resistance in Small-Cell Lung Cancer. *Clin Cancer Res* (2018) 24:2148–58. doi: 10.1158/1078-0432.CCR-17-1932
 8. Chan JM, Quintanal-Villalonga A, Gao VR, Xie Y, Allaj V, Chaudhary O, et al. Signatures of Plasticity, Metastasis, and Immunosuppression in an Atlas of Human Small Cell Lung Cancer. *Cancer Cell* (2021) 39:1479–96.e1418. doi: 10.1016/j.ccell.2021.09.008
 9. Ouadah Y, Rojas ER, Riordan DP, Capostagno S, Kuo CS, Krasnow MA. Rare Pulmonary Neuroendocrine Cells Are Stem Cells Regulated by Rb, P53, and Notch. *Cell* (2019) 179:403–16.e423. doi: 10.1016/j.cell.2019.09.010
 10. Butti R, Das S, Gunasekaran VP, Yadav AS, Kumar D, Kundu GC. Receptor Tyrosine Kinases (RTKs) in Breast Cancer: Signaling, Therapeutic Implications and Challenges. *Mol Cancer* (2018) 17:34. doi: 10.1186/s12943-018-0797-x
 11. Feinberg AP, Koldobskiy MA, Göndör A. Epigenetic Modulators, Modifiers and Mediators in Cancer Aetiology and Progression, Nature Reviews. *Genetics* (2016) 17:284–99. doi: 10.1038/nrg.2016.13
 12. French R, Pauklin S. Epigenetic Regulation of Cancer Stem Cell Formation and Maintenance. *Int J Cancer* (2021) 148:2884–97. doi: 10.1002/ijc.33398
 13. Wei X, Guo J, Li Q, Jia Q, Jing Q, Li Y, et al. Bach1 Regulates Self-Renewal and Impedes Mesendodermal Differentiation of Human Embryonic Stem Cells. *Sci Adv* (2019) 5:eau7887. doi: 10.1126/sciadv.aau7887
 14. Jin J, Liu J, Chen C, Liu Z, Jiang C, Chu H, et al. The Deubiquitinase USP21 Maintains the Stemness of Mouse Embryonic Stem Cells via Stabilization of Nanog. *Nat Commun* (2016) 7:13594. doi: 10.1038/ncomms13594
 15. Li F, Hu Q, He T, Xu J, Yi Y, Xie S, et al. The Deubiquitinase USP4 Stabilizes Twist1 Protein to Promote Lung Cancer Cell Stemness. *Cancers* (2020) 12(6):1582. doi: 10.3390/cancers12061582
 16. Liu G, Guo W, Qin J, Lin Z. OTUB2 Facilitates Tumorigenesis of Gastric Cancer Through Promoting KDM1A-Mediated Stem Cell-Like Properties. *Front Oncol* (2021) 11:711735. doi: 10.3389/fonc.2021.711735
 17. Wu Y, Zhang Y, Liu C, Zhang Y, Wang D, Wang S, et al. Amplification of USP13 Drives non-Small Cell Lung Cancer Progression Mediated by AKT/ MAPK Signaling. *Biomed Pharmacother = Biomed Pharmacother* (2019) 114:108831. doi: 10.1016/j.biopha.2019.108831
 18. Giron P, Eggermont C, Noeparast A, Vandenplas H, Teugels E, Forsyth R, et al. Targeting USP13-Mediated Drug Tolerance Increases the Efficacy of EGFR Inhibition of Mutant EGFR in non-Small Cell Lung Cancer. *Int J Cancer* (2020) 148:2579–93. doi: 10.1002/ijc.33404
 19. Pandey PR, Xing F, Sharma S, Watabe M, Pai SK, Iizumi-Gairani M, et al. Elevated Lipogenesis in Epithelial Stem-Like Cell Confers Survival Advantage in Ductal Carcinoma *in Situ* of Breast Cancer. *Oncogene* (2013) 32:5111–22. doi: 10.1038/ncr.2012.519
 20. Zhang M, Peng R, Wang H, Yang Z, Zhang H, Zhang Y, et al. Nanog Mediated by FAO/ACLY Signaling Induces Cellular Dormancy in Colorectal Cancer Cells. *Cell Death Dis* (2022) 13:159. doi: 10.1038/s41419-022-04606-1
 21. Li J, Condello S, Thomes-Pepin J, Ma X, Xia Y, Hurley TD, et al. Lipid Desaturation Is a Metabolic Marker and Therapeutic Target of Ovarian Cancer Stem Cells. *Cell Stem Cell* (2017) 20:303–14.e305. doi: 10.1016/j.stem.2016.11.004
 22. Luo H, Chen CY, Li X, Zhang X, Su CW, Liu Y, et al. Increased Lipogenesis is Critical for Self-Renewal and Growth of Breast Cancer Stem Cells: Impact of Omega-3 Fatty Acids. *Stem Cells (Dayton Ohio)* (2021) 39:1660–70. doi: 10.1002/stem.3452
 23. Liu T, Zhou T, Luo F, Yang Y, Zhao S, Huang Y, et al. Clinical Significance of Kinetics of Low-Density Lipoprotein Cholesterol and Its Prognostic Value in Limited Stage Small Cell Lung Cancer Patients. *Cancer Control: J Moffitt Cancer Center* (2021) 28:10732748211028257. doi: 10.1177/10732748211028257
 24. Fernández LP, Merino M, Colmenarejo G, Moreno Rubio J, González Pessolani T, Reglero G, et al. Metabolic Health Together With a Lipid Genetic Risk Score Predicts Survival of Small Cell Lung Cancer Patients. *Cancers* (2021) 13(5):1112. doi: 10.3390/cancers13051112
 25. Cristea S, Coles GL, Hornburg D, Gershkovitz M, Arand J, Cao S, et al. The MEK5-ERK5 Kinase Axis Controls Lipid Metabolism in Small-Cell Lung Cancer. *Cancer Res* (2020) 80:1293–303. doi: 10.1158/0008-5472.CAN-19-1027
 26. Peng F, Wang JH, Fan WJ, Meng YT, Li MM, Li TT, et al. Glycolysis Gatekeeper PDK1 Reprograms Breast Cancer Stem Cells Under Hypoxia. *Oncogene* (2018) 37:1062–74. doi: 10.1038/ncr.2017.368
 27. Nguyen HP, Daniel PM, Filiz G, Mantamadiotis T. Investigating Neural Stem Cell and Glioma Stem Cell Self-Renewal Potential Using Extreme Limiting Dilution Analysis (ELDA). *Bio-protocol* (2018) 8:e2991. doi: 10.21769/BioProtoc.2991
 28. Hu Y, Smyth GK. ELDA: Extreme Limiting Dilution Analysis for Comparing Depleted and Enriched Populations in Stem Cell and Other Assays. *J Immunol Methods* (2009) 347:70–8. doi: 10.1016/j.jim.2009.06.008
 29. Shao F, Yang X, Wang W, Wang J, Guo W, Feng X, et al. Associations of PGK1 Promoter Hypomethylation and PGK1-Mediated PDHK1 Phosphorylation With Cancer Stage and Prognosis: A TCGA Pan-Cancer Analysis. *Cancer Commun (Lond)* (2019) 39:54. doi: 10.1186/s40880-019-0401-9
 30. Yang X, Shao F, Shi S, Feng X, Wang W, Wang Y, et al. Prognostic Impact of Metabolism Reprogramming Markers Acetyl-CoA Synthetase 2 Phosphorylation and Ketohexokinase-A Expression in Non-Small-Cell Lung Carcinoma. *Front Oncol* (2019) 9:1123. doi: 10.3389/fonc.2019.01123
 31. Lee JH, Liu R, Li J, Zhang C, Wang Y, Cai Q, et al. Stabilization of Phosphofructokinase 1 Platelet Isoform by AKT Promotes Tumorigenesis. *Nat Commun* (2017) 8:949. doi: 10.1038/s41467-017-00906-9
 32. Sarvi S, Mackinnon AC, Avlonitis N, Bradley M, Rintoul RC, Rassl DM, et al. CD133+ Cancer Stem-Like Cells in Small Cell Lung Cancer are Highly Tumorigenic and Chemo-resistant But Sensitive to a Novel Neuropeptide Antagonist. *Cancer Res* (2014) 74:1554–65. doi: 10.1158/0008-5472.CAN-13-1541
 33. Yi M, Li J, Chen S, Cai J, Ban Y, Peng Q, et al. Emerging Role of Lipid Metabolism Alterations in Cancer Stem Cells. *J Exp Clin Cancer Res: CR* (2018) 37:118. doi: 10.1186/s13046-018-0784-5
 34. Loomba R, Mohseni R, Lucas KJ, Gutierrez JA, Perry RG, Trotter JF, et al. TVB-2640 (FASN Inhibitor) for the Treatment of Nonalcoholic Steatohepatitis: FASCINATE-1, A Randomized, Placebo-Controlled Phase 2a Trial. *Gastroenterology* (2021) 161:1475–86. doi: 10.1053/j.gastro.2021.07.025
 35. Syed-Abdul MM, Parks EJ, Gaballah AH, Bingham K, Hammoud GM, Kemble G, et al. Fatty Acid Synthase Inhibitor TVB-2640 Reduces Hepatic De Novo Lipogenesis in Males With Metabolic Abnormalities. *Hepatology (Baltimore Md.)* (2020) 72:103–18. doi: 10.1002/hep.31000
 36. Falchook G, Infante J, Arkenau HT, Patel MR, Dean E, Borazanci E, et al. First-In-Human Study of the Safety, Pharmacokinetics, and Pharmacodynamics of First-in-Class Fatty Acid Synthase Inhibitor TVB-2640 Alone and With a Taxane in Advanced Tumors. *EclinicalMedicine* (2021) 34:100797. doi: 10.1016/j.eclinm.2021.100797
 37. Puig T, Aguilar H, Cufi S, Oliveras G, Turrado C, Ortega-Gutiérrez S, et al. A Novel Inhibitor of Fatty Acid Synthase Shows Activity Against HER2+ Breast Cancer Xenografts and is Active in Anti-HER2 Drug-Resistant Cell Lines. *Breast Cancer Res: BCR* (2011) 13:R131. doi: 10.1186/bcr3077
 38. Shen W, Zhang W, Ye W, Wang H, Zhang Q, Shen J, et al. SR9009 Induces a REV-ERB Dependent Anti-Small-Cell Lung Cancer Effect Through Inhibition of Autophagy. *Theranostics* (2020) 10:4466–80. doi: 10.7150/thno.42478
 39. Zhang J, Zhang P, Wei Y, Piao HL, Wang W, Maddika S, et al. Deubiquitylation and Stabilization of PTEN by USP13. *Nat Cell Biol* (2013) 15:1486–94. doi: 10.1038/ncb2874
 40. Han C, Yang L, Choi HH, Baddour J, Achreja A, Liu Y, et al. Amplification of USP13 Drives Ovarian Cancer Metabolism. *Nat Commun* (2016) 7:13525. doi: 10.1038/ncomms13525
 41. Zhang S, Zhang M, Jing Y, Yin X, Ma P, Zhang Z, et al. Deubiquitinase USP13 Dictates MCL1 Stability and Sensitivity to BH3 Mimetic Inhibitors. *Nat Commun* (2018) 9:215. doi: 10.1038/s41467-017-02693-9
 42. Fang X, Zhou W, Wu Q, Huang Z, Shi Y, Yang K, et al. Deubiquitinase USP13 Maintains Glioblastoma Stem Cells by Antagonizing FBXL14-Mediated Myc Ubiquitination. *J Exp Med* (2017) 214:245–67. doi: 10.1084/jem.20151673
 43. Santos CR, Schulze A. Lipid Metabolism in Cancer. *FEBS J* (2012) 279:2610–23. doi: 10.1111/j.1742-4658.2012.08644.x
 44. Menendez JA, Lupu R. Fatty Acid Synthase and the Lipogenic Phenotype in Cancer Pathogenesis, Nature Reviews. *Cancer* (2007) 7:763–77. doi: 10.1038/nrc2222

45. Jones SF, Infante JR. Molecular Pathways: Fatty Acid Synthase. *Clin Cancer Res* (2015) 21:5434–8. doi: 10.1158/1078-0432.CCR-15-0126
46. Gouw AM, Eberlin LS, Margulis K, Sullivan DK, Toal GG, Tong L, et al. Oncogene KRAS Activates Fatty Acid Synthase, Resulting in Specific ERK and Lipid Signatures Associated With Lung Adenocarcinoma. *Proc Natl Acad Sci U S A* (2017) 114:4300–5. doi: 10.1073/pnas.1617709114
47. Ali A, Levantini E, Teo JT, Goggi J, Clohessy JG, Wu CS, et al. Fatty Acid Synthase Mediates EGFR Palmitoylation in EGFR Mutated non-Small Cell Lung Cancer. *EMBO Mol Med* (2018) 10(3):e8313. doi: 10.15252/emmm.201708313
48. Ventura R, Mordec K, Waszczuk J, Wang Z, Lai J, Fridlib M, et al. Inhibition of *De Novo* Palmitate Synthesis by Fatty Acid Synthase Induces Apoptosis in Tumor Cells by Remodeling Cell Membranes, Inhibiting Signaling Pathways, and Reprogramming Gene Expression. *EBioMedicine* (2015) 2:808–24. doi: 10.1016/j.ebiom.2015.06.020
49. Lyu Q, Zhu W, Wei T, Ding W, Cao M, Wang Q, et al. High Mutations in Fatty Acid Metabolism Contribute to a Better Prognosis of Small-Cell Lung Cancer Patients Treated With Chemotherapy. *Cancer Med* (2021) 10:7863–76. doi: 10.1002/cam4.4290

Conflict of Interest: The authors declare that the research was conducted in the absence of any commercial or financial relationships that could be construed as a potential conflict of interest.

Publisher's Note: All claims expressed in this article are solely those of the authors and do not necessarily represent those of their affiliated organizations, or those of the publisher, the editors and the reviewers. Any product that may be evaluated in this article, or claim that may be made by its manufacturer, is not guaranteed or endorsed by the publisher.

Copyright © 2022 Wang, Lin, Li, Cheng, Sun, Shao, Yang, Zhang, Feng, Gao, Gao and He. This is an open-access article distributed under the terms of the Creative Commons Attribution License (CC BY). The use, distribution or reproduction in other forums is permitted, provided the original author(s) and the copyright owner(s) are credited and that the original publication in this journal is cited, in accordance with accepted academic practice. No use, distribution or reproduction is permitted which does not comply with these terms.